Inorg. Chem. **2002**, *41*, 5544–5554

Preparation of Highly Efficient Manganese Catalase Mimics[||]

Michael U. Triller,[†] Wen-Yuan Hsieh,[‡] Vincent L. Pecoraro,*[,‡] Annette Rompel,[§] and Bernt Krebs*[,†]

Institut für Anorganische und Analytische Chemie der Westfälischen Wilhelms-Universität Münster, Wilhelm-Klemm-Str. 8, 48149 Münster, Germany, Institut für Biochemie der Westfälischen Wilhelms-Universität Münster, Wilhelm-Klemm-Str. 2, 48149 Münster, Germany, and Department of Chemistry, The University of Michigan, Ann Arbor, Michigan 48109-1055

Received July 24, 2002

The series of compounds $[Mn(bpia)(\mu\text{-}OAc)]_2(ClO_4)_2$ (**1**), $[Mn_2(bpia)_2(\mu O)(\mu\text{-}OAc)](ClO_4)_3 \cdot CH_3CN$ (**2**), $[Mn(bpia)(\mu\text{-}O)]_2(ClO_4)_2(PF_6) \cdot 2CH_3CN$ (**3**), $[Mn(bpia)(Cl)_2](ClO)_4$ (**4**), and $[(Mn(bpia)(Cl))_2(\mu\text{-}O)](ClO_4)_2 \cdot 2CH_3CN$ (**5**) (bpia = bis-(picolyl)(*N*-methylimidazol-2-yl)amine) represents a structural, spectroscopic, and functional model system for manganese catalases. Compounds **3** and **5** have been synthesized from **2** via bulk electrolysis and ligand exchange, respectively. All complexes have been structurally characterized by X-ray crystallography and by UV–vis and EPR spectroscopies. The different bridging ligands including the rare mono-μ-oxo and mono-μ-oxo-mono-μ-carboxylato motifs lead to a variation of the Mn–Mn separation across the four binuclear compounds of 1.50 Å ($Mn_2^{II,II}$ = 4.128 Å, $Mn_2^{III,III}$ = 3.5326 and 3.2533 Å, $Mn_2^{III,IV}$ = 2.624 Å). Complexes **1**, **2**, and **3** are mimics for the $Mn_2^{II,II}$, the $Mn_2^{III,III}$, and the $Mn_2^{III,IV}$ oxidation states of the native enzyme. UV–vis spectra of these compounds show similarities to those of the corresponding oxidation states of manganese catalase from *Thermus thermophilus* and *Lactobacillus plantarum*. Compound **2** exhibits a rare example of a Jahn–Teller compression. While complexes **1** and **3** are efficient catalysts for the disproportionation of hydrogen peroxide and contain an N_4O_2 donor set, **4** and **5** show no catalase activity. These complexes have an N_4Cl_2 and N_4OCl donor set, respectively, and serve as mimics for halide inhibited manganese catalases. Cyclovoltammetric data show that the substitution of oxygen donor atoms with chloride causes a shift of redox potentials to more positive values. To our knowledge, complex **1** is the most efficient binuclear functional manganese catalase mimic exhibiting saturation kinetics to date.

Introduction

It is now well recognized that enzymes containing manganese cofactors are widespread. In addition to the tetranuclear manganese cluster found in the oxygen evolving complex,[1] there are numerous enzymes[2] that contain mononuclear (e.g., superoxide dismutase[3] and manganese dioxygenase[4]) or binuclear (e.g., catalases,[5−7] ribonucleotide reductase,[8] arginase[9]) manganese centers. Often, these mono- and binuclear manganese enzymes exhibit activities that are similar to iron enzymes, with active sites, in a few cases such as superoxide dismutases or ribonucleotide reductases, that appear remarkably similar. Therefore, an understanding of manganese enzymes not only furthers our appreciation for the biological chemistry of this element but also provides a broader foundation for the understanding of metalloenzymology.

[||] Dedicated to Prof. Dr. Dr. h.c. mult. Achim Müller on the occasion of his 65th birthday.

* Authors to whom correspondence should be addressed. E-mail: krebs@uni-muenster.de (B.K.); vlpec@umich.edu (V.L.P.).

[†] Institut für Anorganische und Analytische Chemie der Westfälischen Wilhelms-Universität Münster.

[‡] Department of Chemistry, University of Michigan.

[§] Institut für Biochemie der Westfälischen Wilhelms-Universität Münster.

(1) Zouni, A.; Witt, H. T.; Kern, J.; Fromme, P.; Krauss, N.; Saenger, W.; Orth, P. *Nature* **2001**, *409*, 739.
(2) Law, N. A.; Caudle, M. T.; Pecoraro, V. L. *Adv. Inorg. Chem.* **1999**, *46*, 305.
(3) Whittaker, J. W. In *Metal Ions in Biological Systems*; Sigel, A., Sigel, H., Eds.; Marcel Dekker: New York, 2000; Vol. 37, p 587.
(4) Que, L., Jr.; Reynolds, M. F. In *Metal Ions in Biological Systems*; Sigel, A., Sigel, H., Eds.; Marcel Dekker: New York, 2000; Vol. 37, p 505.
(5) (a) Kono, Y.; Fridovich, I. *J. Biol. Chem.* **1983**, *258*, 6015. (b) Beyer, W. F., Jr.; Fridovich, I. *Biochemistry* **1985**, *24*, 6460.
(6) (a) Barynin, V. V.; Vagin, A. A.; Melik-Adamyan, W. R.; Grebenko, A. I.; Khangulov, S. V.; Popov, A. N.; Andrianova, M. E.; Vainshtein, B. K. *Dokl. Akad. Nauk.* **1986**, *288*, 877. (b) Barynin, V. V.; Hempstead, P. D.; Vagin, A. A.; Antonyuk, S. V.; Melik-Adamyan, W. R.; Lamzin, V. S.; Harrison, P. M.; Artymyuk, P. J. *J. Inorg. Biochem.* **1997**, *67*, 196.
(7) Allgood, G. S.; Perry, J. J. *J. Bacteriol.* **1986**, *168*, 563.
(8) Auling, G.; Follmann, H. In *Metal Ions in Biological Systems*; Sigel, A., Sigel, H., Eds.; Marcel Dekker: New York, 1994; Vol. 30, p 131.
(9) Ash, D. E.; Cox, J. D.; Christianson, D. W. In *Metal Ions in Biological Systems*; Sigel, A., Sigel, H., Eds.; Marcel Dekker: New York, 2000; Vol. 37, p 407.

10.1021/ic025897a CCC: $22.00
Published on Web 09/17/2002

The manganese catalases are the most intensively studied binuclear manganese enzymes. Catalases are enzymes that protect cells from deleterious effects caused by hydrogen peroxide, a byproduct of respiration, by disproportionating H_2O_2 into water and dioxygen. Besides heme type catalases[10] and particular enzymes such as chloroperoxidase that disproportionate hydrogen peroxide in addition to peroxidase activity,[11] there is the class of manganese catalases that has been found in the three bacterial organisms *Lactobacillus plantarum*,[5] *Thermus thermophilus*,[6] and *Thermoleophilum album*.[7] Manganese catalase from *Thermus thermophilus* is best characterized structurally. A recent X-ray structural analysis at 1 Å resolution[12] of the oxidized form of the enzyme reveals an active site containing two Mn^{III} ions with a 3.13 Å metal to metal distance. The metal centers are bridged by the carboxylate group of a glutamate residue in a syn−syn fashion. Two oxygen atoms complete the bridging motif, the exact structure of which is yet unclear. At least one of the bridging oxygen atoms is thought to be an O^{2-} group, whereas in the reduced $Mn_2^{II,II}$ form both bridging oxygen atoms come from water and/or hydroxide. This triply bridged form has been shown to be in a pH-dependent equilibrium with a species containing a mono-μ-oxo-mono-μ-carboxylato bridge.[13] The coordination sphere around the manganese centers also contains one terminal glutamate and one terminal histidine ligand per manganese and is best described as distorted square pyramidal. Besides the catalytically active $Mn_2^{II,II}$ and $Mn_2^{III,III}$ oxidation states, through which the enzyme cycles during turnover, the inactive $Mn_2^{II,III}$ and $Mn_2^{III,IV}$ oxidation states also can be accessed and transformed into one another by use of various oxidants/reductants. Monovalent ligands with a negative charge like chloride, fluoride, azide, nitrite, and nitrate have been found to inhibit the $Mn_2^{II,II}$ state of the enzyme while cyanide causes no inhibition.[14] So far, only two functional model systems have been described which employ the $Mn_2^{II,II}$ and $Mn_2^{III,III}$ oxidation states in their catalytic cycles. The first system, $[Mn_2(L^1)(\mu\text{-OAc})]^{2+}$, is based on the heptadentate ligand L^1 = *N*,*N*,*N*′,*N*′-tetrakis(2-methylenebenzimidazolyl)-1,3-diaminopropan-2-ol and has been the first functional catalase mimic (Table 3).[15−18] The second system is the $[Mn_2(2\text{-OHsalpn})_2]$ system, which has been crystallographically and spectroscopically fully characterized in four different oxidation states, and serves as both a structural and functional manganese catalase mimic (Table 3).[19−21] Like the aforementioned heptadentate ligand, the pentadentate 2-OH-salpn ligand offers preorganized binding sites for two metal ions and is therefore tailor-made for the synthesis of binuclear complexes. To have a greater variety of possible bridging motifs available for a manganese catalase model system, we chose to utilize the ligand bpia (bis(picolyl)(*N*-methylimidazol-2-yl)amine) that belongs to the class of tripodal ligands.[22,23] When coordinating to a metal center, tripodal ligands form complexes leaving two vacant coordination sites in cis position to each other. These vacant coordination sites facilitate the synthesis of binuclear complexes while at the same time they allow control over the bridging ligands.

In this paper, we report the synthesis, characterization, and catalase activity of the novel complexes $[Mn(bpia)(\mu\text{-OAc})]_2(ClO_4)_2$ (**1**), $[Mn_2(bpia)_2(\mu\text{-O})(\mu\text{-OAc})](ClO_4)_3\cdot CH_3CN$ (**2**), $[Mn(bpia)(\mu\text{-O})]_2(ClO_4)_2(PF_6)\cdot 2CH_3CN$ (**3**), $[Mn(bpia)(Cl)_2](ClO)_4$ (**4**), and $[(Mn(bpia)(Cl))_2(\mu\text{-O})](ClO_4)_2\cdot 2CH_3CN$ (**5**). Compounds **1**, **2**, and **3** are structural mimics of the $Mn_2^{II,II}$, $Mn_2^{III,III}$, and $Mn_2^{III,IV}$ forms of manganese catalase. It will be shown that **1** is the most efficient functional catalase mimic with saturation kinetics observed. Complex **3**, although being a structural model for the inactive form of the enzyme, also catalytically disproportionates hydrogen peroxide, while **2** is oxidized to **3** by hydrogen peroxide. Attempts to synthesize model compounds for the anion inhibited form of manganese catalase yielded complexes **4** and **5**, which show no catalytic activity with respect to the disproportionation of hydrogen peroxide.

Experimental Section

Physical Measurements. IR spectra were recorded on a Perkin-Elmer Spectrum GX FT-IR spectrometer and a Bruker IFS 48 spectrometer in the range 4000−400 cm^{-1}. Samples were prepared as KBr disks. Elemental analyses were carried out on a Perkin-Elmer 2400 Series 2 analyzer, an Elementar vario EL III analyzer, and a Heraeus CHN-O-Rapid analyzer. UV−vis spectra were measured at 25 °C on a Hewlett-Packard 8453 diode array spectrometer using quartz cuvettes (1 cm) and acetonitrile as solvent. The concentration of the samples was $c = 5\cdot 10^{-4}$ mol·L^{-1}. EPR spectra were recorded on a Bruker EMX EPR spectrometer at X-band frequency. For low-temperature spectra, an Oxford Instruments continuous flow helium cryostat and a temperature control system were used. Cyclic voltammetry experiments for compounds **2**−**5** were carried out in acetonitrile on a BAS CV-27 voltammograph equipped with a BAS C-1B cell stand and a BAS RXY recorder. For compound **1**, *N*,*N*-dimethylformamide was used. The concentration of all samples was $c = 1\cdot 10^{-3}$ mol·L^{-1}. Prior to use, solvents were purified by standard literature methods. Tetrabutylammonium hexafluorophosphate (recrystallized from ethanol) was used as supporting electrolyte at a concentration of 0.1 mol·L^{-1}. A three electrode array consisting of a glassy carbon working

(10) Maté, M. J.; Murshudov, G.; Bravo, J.; Melik-Adamyan, W.; Loewen, P. C.; Fita, I. In *Handbook of Metalloproteins*; Messerschmidt, A., Huber, R., Poulos, T., Wieghardt, K., Eds.; John Wiley & Sons, LTD: New York, 2001; pp 486−502.
(11) Thomas, J. A.; Morris, D. R.; Hager, L. P. *J. Biol. Chem.* **1970**, *245*, 3129.
(12) Antonyuk, S. V.; Melik-Adamyan, W. R.; Popov, A. N.; Lamzin, V. S.; Hempstead, P. D.; Harrison, P. M.; Artymyuk, P. J.; Barynin, V. V. *Crystallogr. Rep. (Transl. Kristallografiya)* **2000**, *45*, 105.
(13) Michaud-Soret, I.; Jacquamet, L.; Debaecker-Petit, N.; Le Pape, L.; Barynin, V. V.; Latour, J.-M. *Inorg. Chem.* **1998**, *37*, 3874.
(14) Khangulov, S. V.; Barynin, V. V.; Voevodskaya, N. V. *Biochim. Biophys. Acta* **1990**, *1020*, 305.
(15) Boelrijk, A. E. M.; Dismukes, G. C. *Inorg. Chem.* **2000**, *39*, 3020.
(16) Mathur, P.; Crowder, M.; Dismukes, G. C. *J. Am. Chem. Soc.* **1987**, *109*, 5227.
(17) Pessiki, P. J.; Khangulov, S. V.; Ho, D. M.; Dismukes, G. C. *J. Am. Chem. Soc.* **1994**, *116*, 891.
(18) Pessiki, P. J.; Dismukes, G. C. *J. Am. Chem. Soc.* **1994**, *116*, 898.
(19) Gelasco, A.; Bensiek, S.; Pecoraro, V. L. *Inorg. Chem.* **1998**, *37*, 3301.
(20) Gelasco, A.; Pecoraro, V. L. *J. Am. Chem. Soc.* **1993**, *115*, 7928.
(21) Gelasco, A.; Kirk, M. L.; Kampf, J. W.; Pecoraro, V. L. *Inorg. Chem.* **1997**, *36*, 1829.
(22) Pascaly, M.; Duda, M.; Rompel, A.; Sift, B. H.; Meyer-Klaucke, W.; Krebs, B. *Inorg. Chim. Acta* **1999**, *291*, 289.
(23) (a) Wei, N.; Murthy, N. N.; Tyeklár, Z.; Karlin, K. D. *Inorg. Chem.* **1994**, *33*, 1177. (b) Reese, C. B.; Pei-Zhou, Z. *J. Chem. Soc., Perkin Trans.* **1993**, 2291.

Table 1. Crystal Data and X-ray Experimental Parameters for Complexes **1**−**5**

	1	**2**	**3**	**4**	**5**
formula	$C_{38}H_{44}N_{10}Cl_2O_{12}Mn_2$	$C_{38}H_{44}N_{11}Cl_3Mn_2O_{15}$	$C_{38}H_{44}N_{12}Cl_2F_6O_{10}Mn_2P_1$	$C_{17}H_{19}N_5Cl_3Mn_1O_4$	$C_{38}H_{44}N_{12}Cl_4Mn_2O_9$
M (g·mol^{-1})	1013.61	1111.07	1154.60	518.66	1064.53
cryst syst	triclinic	monoclinic	monoclinic	monoclinic	monoclinic
space group	$P\bar{1}$	$P2_1/n$	$P2_1/n$	Cc	$P2_1/c$
T (K)	158(2)	158(2)	158(2)	153(2)	213(2)
a (Å)	7.892(2)	10.746(2)	15.373(3)	7.971(2)	10.445(2)
b (Å)	10.706(2)	22.423(4)	10.442(2)	22.218(4)	14.277(3)
c (Å)	14.051(3)	20.143(4)	16.210(3)	11.875(2)	15.123(3)
α (deg)	107.79(3)	90	90	90	90
β (deg)	100.10(3)	100.49(3)	114.91(3)	98.99(3)	90.71(3)
γ (deg)	94.12(3)	90	90	90	90
V (Å^3)	1102.9(4)	4773(2)	2360.0(8)	2077.2(7)	2255.0(8)
Z	1	4	2	4	2
D_{calcd} (g·cm^{-3})	1.526	1.546	1.625	1.658	1.568
μ (mm^{-1})	0.766	0.775	0.775	1.057	0.864
R1[a]	0.0367	0.0448	0.0678	0.0381	0.0477
wR2[b]	0.1055	0.1246	0.1490	0.0799	0.0988
GOF[c]	1.078	1.085	0.840	1.021	1.020

[a] $R1 = \sum||F_{obsd}| - |F_{calcd}||/\sum|F_{obsd}|$. [b] $wR2 = \{\sum[w(F_{obsd}^2 - F_{calcd}^2)^2]/\sum[w(F_{obsd}^2)^2]\}^{1/2}$. [c] $GOF = \{\sum[w(F_{obsd}^2 - F_{calcd}^2)^2]/n_{data} - n_{vari}\}^{1/2}$.

electrode, a platinum wire counter electrode, and a $Ag/AgNO_3$ reference electrode, prepared in acetonitrile (0.1 mol·L^{-1} Bu_4NPF_6, 0.01 mol·L^{-1} $AgNO_3$), was used. Using the described conditions, the ferrocene/ferrocinium redox couple was observed at $E_{1/2} = 0.41$ V versus SCE and at $E_{1/2} = 0.10$ V versus $Ag/AgNO_3$. For bulk electrolysis, a platinum mesh was used as working electrode along with a platinum disk as counter electrode and a silver wire as reference electrode.

Kinetic Measurements. Catalase activities of complexes **1** (in *N*-methylformamide) and **3** (in acetonitrile) were measured at 25 °C on the basis of fluorescence quenching using an oxygen sensor.[24] Complex **2** is oxidized stoichiometrically by hydrogen peroxide (monitored by UV−vis, data not shown here). Hydrogen peroxide solution in acetonitrile (for **3**) and *N*-methylformamide (for **1**), respectively, was placed in a vessel equipped with a thermostat (5 mL, prepared in different concentrations from 35.9% hydrogen peroxide solution in water, concentration determined iodometrically and manganometrically). Before each measurement, a calibration of the oxygen sensor was carried out by saturating the solution with air (100% dioxygen) and then with argon (0% dioxygen). The dioxygen concentration in air-saturated acetonitrile (*N*-methylformamide) has been determined to be 2.42 mmol·L^{-1} (1.31 mmol·L^{-1}).[25] After a baseline had been established, 0.1 mL of a 0.01 molar solution of complex in degassed solvent (vide supra) was added, and the oxygen evolution was monitored. The average initial rate over three independent measurements, expressed as mol H_2O_2·s^{-1}·(mol catalyst)$^{-1}$,[18] was determined by linear regression from the slope of the concentration versus time plots.

X-ray Crystallography. Unless otherwise stated, all structures were solved by direct methods using the program system SHELXS97.[26] All other non-hydrogen atoms were taken from a series of full-matrix least-squares refinement cycles based on F^2 with the SHELXL 97 program followed by difference Fourier synthesis.[26] All hydrogen atoms were placed on calculated positions and allowed to ride on their corresponding carbon atoms with isotropic thermal parameters for the methyl protons 1.5 times the value for U_{eq} of the bonding atom and all other hydrogen atoms 1.2 times the value for U_{eq} of the bonding atom. All non-hydrogen atoms were refined anisotropically.

[Mn(bpia)(μ-OAc)]$_2$(ClO$_4$)$_2$ (1). Single crystals were obtained by vapor diffusion of diethyl ether into a methanol solution of **1**. A block shaped yellow crystal of dimensions 0.42 × 0.40 × 0.40 mm^3 was chosen and mounted onto a Siemens Smart 1K CCD diffractometer. Unit cell data and diffraction intensities were collected at 158 K using Mo Kα radiation (graphite monochromated, $\lambda = 0.71073$ Å). Further crystal data and experimental parameters are listed in Table 1.

The structure was solved by a Patterson synthesis using the program system SHELXS 97.[26]

[Mn$_2$(bpia)$_2$(μ-O)(μ-OAc)](ClO$_4$)$_3$·CH$_3$CN (2). Single crystals were obtained by vapor diffusion of diethyl ether into an acetonitrile solution of **2**. A rectangular red crystal of dimensions 0.44 × 0.26 × 0.24 mm^3 was chosen and mounted onto a Siemens Smart 1K CCD diffractometer. Unit cell data and diffraction intensities were collected at 158 K using Mo Kα radiation (graphite monochromated, $\lambda = 0.71073$ Å). Further crystal data and experimental parameters are listed in Table 1.

One perchlorate ion is disordered. The disorder can be described as a rotation around the Cl(1)−O(6) axis by approximately 20°. The occupation factors for both forms were refined to 0.61 and 0.39, respectively.

[Mn(bpia)(μ-O)]$_2$(ClO$_4$)$_2$(PF$_6$)·2CH$_3$CN (3). Single crystals were obtained by vapor diffusion of diethyl ether into an acetonitrile solution of **3**. A plate shaped green crystal of dimensions 0.20 × 0.10 × 0.02 mm^3 was chosen and mounted onto a Siemens Smart 1K CCD diffractometer. Unit cell data and diffraction intensities were collected at 158 K using Mo Kα radiation (graphite monochromated, $\lambda = 0.71073$ Å). Further crystal data and experimental parameters are listed in Table 1. The poor data are caused by bad crystal quality.

[Mn(bpia)(Cl)$_2$](ClO)$_4$ (4). Single crystals were obtained by vapor diffusion of diethyl ether into an acetonitrile solution of **4**. A rectangular deep red crystal of dimensions 0.33 × 0.27 × 0.17 mm^3 was chosen and mounted onto a Bruker AXS Smart APEX diffractometer. Unit cell data and diffraction intensities were collected at 173 K using Mo Kα radiation (graphite monochromated, $\lambda = 0.71073$ Å). Further crystal data and experimental parameters are listed in Table 1.

[(Mn(bpia)(Cl))$_2$(μ-O)](ClO$_4$)$_2$·2CH$_3$CN (5). Single crystals were obtained by vapor diffusion of diethyl ether into an acetonitrile

(24) Könecke, R.; Comte, A.; Jürgens, H.; Kohls, O.; Lam, H.; Scheper, T. *Chem. Ing. Tech.* **1998**, *70*, 1611.
(25) Franco, C.; Olmsted, J., III. *Talanta* **1990**, *37*, 905.
(26) (a) Sheldrick, G. M. *SHELXS97*; University of Göttingen: Göttingen, Germany, 1997. (b) Sheldrick, G. M. *SHELXL97*, University of Göttingen: Göttingen, Germany, 1997.

solution of **5**. A rectangular green crystal of dimensions 0.40 × 0.40 × 0.32 mm^3 was chosen and mounted onto a STOE imaging plate diffraction system. Unit cell data and diffraction intensities were collected at 213 K using Mo Kα radiation (graphite monochromated, $\lambda = 0.71073$ Å). The sample to plate distance was fixed at 70 mm with a scan range of $0° \le \varphi \le 200°$. The exposure time was 3 min, and the oscillating angle $\Delta\varphi = 1.1°$. Further crystal data and experimental parameters are listed in Table 1.

The perchlorate ion is disordered. The disorder can be described as a rotation around the Cl(2)−O(4) axis by approximately 22°. The occupation factors for both forms were refined to 0.65 and 0.35, respectively.

Syntheses. The ligand bpia (bis(picolyl)(*N*-methylimidazol-2-yl)amine) was synthesized according to previously reported methods.[22,23] All reagents used in the syntheses were purchased from Aldrich and Fluka and used without further purification. All solvents were of analytical grade and used without further purification unless stated otherwise.

Caution! *Perchlorate salts of compounds containing organic ligands are potentially explosive. Only small quantities of these compounds should be prepared, and suitable precautionary measures should be taken when they are handled.*

[Mn(bpia)(μ-OAc)]$_2$(ClO$_4$)$_2$ (1). The complex was prepared by reacting equimolar amounts of bpia (0.2 mmol, 59 mg) and Mn(OAc)$_2$·4H$_2$O (0.2 mmol, 49 mg) in methanol. The resulting pale yellow solution was stirred for 30 min, and then NaClO$_4$·H$_2$O (0.2 mmol, 28 mg) was added and the resulting reaction mixture stirred for another 30 min. Vapor diffusion of diethyl ether into this solution yielded yellow crystals suitable for X-ray diffraction. Yield: 81 mg, 40%. Anal. Calcd for $C_{38}H_{44}N_{10}Cl_2O_{12}Mn_2$: C, 45.03; H, 4.38; N, 13.82. Found: C, 44.79; H, 4.34; N, 13.74. IR (KBr, cm^{-1}): 3420(br), 3121(w), 1602(vs), 1576(vs), 1507(s), 1481(s), 1442(vs), 1279(m), 1092 (vs), 1015(s), 950(m), 905(m), 762(s), 656(m), 636(s), 623(s).

[Mn$_2$(bpia)$_2$(μ-O)(μ-OAc)](ClO$_4$)$_3$·CH$_3$CN (2). The complex was synthesized by slight modification of a previously published procedure.[27] Bpia (0.2 mmol, 59 mg) was dissolved in a methanol/ethanol mixture (1:1), and Mn(OAc)$_3$·2H$_2$O (0.2 mmol, 54 mg) was added as a solid. The resulting reddish brown reaction mixture was stirred for 2 h and then filtered to remove small amounts of unreacted starting material. To the filtrate, NaClO$_4$·H$_2$O (0.3 mmol, 42 mg) was added. The resulting reddish brown precipitate was filtered and washed with ethanol. Red crystals suitable for X-ray diffraction were grown by vapor diffusion of diethyl ether into an acetonitrile solution of the complex. Yield: 151 mg, 68%. Anal. Calcd for $C_{36}H_{41}N_{10}Cl_3Mn_2O_{15}$: C, 40.41; H, 3.86; N, 13.09. Found: C, 40.40; H, 3.59; N, 13.30. IR (KBr, cm^{-1}): 3427(br), 3132(w), 3079(w), 2919(w), 1607(s), 1512(s), 1484(m), 1444(s), 1356(w), 1311(w), 1286(w), 1095(vs), 976(m), 879(w), 766(s), 665(w), 624(s).

[Mn(bpia)(μ-O)]$_2$(ClO$_4$)$_2$(PF$_6$)·2CH$_3$CN (3). The complex was synthesized from **2** via bulk electrolysis of a 0.1 M solution of **2** in acetonitrile with 0.1 M Bu$_4$NPF$_6$ as supporting electrolyte. The volume of solvent was reduced in a N_2 stream. Upon addition of CH_2Cl_2, a brown precipitate was obtained, which was filtered, washed with methanol, and dissolved in acetonitrile. Green crystals suitable for X-ray diffraction were grown by vapor diffusion of diethyl ether into this solution. Yield: 50 mg, 43%. Anal. Calcd for $C_{38}H_{44}N_{12}Cl_2F_6O_{10}Mn_2P_1$: C, 39.53; H, 3.84; N, 14.56. Found: C, 39.67; H, 3.91; N, 14.39. IR (KBr, cm^{-1}): 3432(br), 1607(s), 1510(s), 1485(m), 1445(s), 1287(w), 1165(m), 1099(s), 1024(w), 977(w), 840(vs), 764(s), 702(w), 665(w), 623(w), 558(vs).

[Mn(bpia)(Cl)$_2$](ClO)$_4$ (4). The complex was prepared by slight modification of a previously published procedure.[28] To a methanol suspension of **2** (0.06 mmol, 68 mg) was added 2 mL of a 0.12 M solution of HCl in acetonitrile. The 0.12 M solution of HCl in acetonitrile was prepared by dilution of 0.1 mL of 12 M aqueous HCl to 10 mL with acetonitrile. Upon addition of the HCl solution, the reddish brown reaction mixture turned into a deep red solution, which was stirred for 5 min and then filtered. Deep red crystals suitable for X-ray diffraction were obtained by vapor diffusion of diethyl ether into the solution. Yield: 40 mg, 64%. Anal. Calcd for $C_{17}H_{19}N_5Cl_3Mn_1O_4$: C, 39.37; H, 3.69; N, 13.50. Found: C, 39.51; H, 3.73; N, 13.20. IR (KBr, cm^{-1}): 3138(m), 2934(w), 1604(s), 1514(s), 1445(s), 1357(w), 1316(m), 1285(m), 1168(s), 1089(vs), 1026(s), 977(m), 885(m), 816(w), 778(s), 761(vs), 665(m), 623(s), 526(m), 440(m).

[(Mn(bpia)(Cl))$_2$(μ-O)](ClO$_4$)$_2$·2CH$_3$CN (5). The complex was prepared by slight modification of a previously published procedure.[28] To a DMF solution of **2** (0.06 mmol, 68 mg) was added 1 mL of a 0.12 M solution of HCl in acetonitrile. The color changed from reddish brown to green. The solution was stirred for 5 min and then filtered. Vapor diffusion of diethyl ether into this solution yielded green crystals which were recrystallized from acetonitrile to give green crystals suitable for X-ray diffraction. Yield: 49 mg, 77%. Anal. Calcd for $C_{34}H_{38}N_{10}Cl_4Mn_2O_9$: C, 41.57; H, 3.90; N, 14.26. Found: C, 41.66; H, 3.88; N, 14.26. IR (KBr, cm^{-1}): 3424(br), 3136(w), 2942(w), 1605(s), 1509(s), 1482(m), 1442(s), 1359(w), 1317(w), 1285(w), 1091(vs), 969(m), 879(s), 762(s), 701(w), 624(s), 525(w).

Results and Discussion

Description of Structures. [Mn(bpia)(μ-OAc)]$_2$(ClO$_4$)$_2$ (1). The crystal structure of the cation in **1** is depicted in Figure 1. Selected bond distances and angles are given in Table 2. Compound **1** crystallizes in the triclinic space group $P\bar{1}$ with one complex cation and two perchlorate counteranions in the unit cell. The two manganese centers in the dication are related by a crystallographic inversion center. They are bridged by two acetato groups in a syn−anti fashion resulting in an intermetal distance of 4.128(1) Å. This is considerably shorter than the distances found in the syn−anti dicarboxylato bridged complexes $[Mn_2(bipy)_4(\mu\text{-}C_2H_5CO_2)_2]^{2+}$ (4.653 Å), $[Mn_2(bipy)_4(\mu\text{-}C_6H_5CO_2)_2]^{2+}$ (4.509 Å), and $[Mn(bipy)_4(\mu\text{-}CH_3O_2)_2]^{2+}$ (4.583 Å).[29−31] Mn−Mn distances similar to that in **1** can be found in two syn−anti diacetato bridged complexes that contain tetradentate nitrogen donor ligands: $[Mn_2(\mu\text{-}CH_3CO_2)_2(bispicMe_2en)_2](ClO_4)_2$ (4.298 Å) (bispicMe$_2$en = *N*,*N*′-dimethyl-*N*,*N*′-bis(2-pyridylmethyl)-ethane-1,2-diamine) and $[Mn_2(\mu\text{-}CH_3CO_2)_2(tpa)_2](TCNQ)_2\cdot 2CH_3CN$ (4.145 Å) (tpa = tris(2-pyridylmethyl)amine, TCNQ = tetracyanoquinodimethane).[32,33] The coordination

(27) Oberhausen, K. J.; O'Brien, R. J.; Richardson, J. F.; Buchanan, R. M.; Costa, R.; Latour, J.-M.; Tsai, H.-S.; Hendrickson, D. N. *Inorg. Chem.* **1993**, *32*, 4561.

(28) Pal, S.; Olmstead, M. M.; Armstrong, W. H. *Inorg. Chem.* **1995**, *34*, 4708.

(29) Zhang, C.; Janiak, C. *Z. Anorg. Allg. Chem.* **2001**, *627*, 1972.

(30) Albela, B.; Corbella, M.; Ribas, J.; Castro, I.; Sletten, J.; Stoeckli-Evans, H. *Inorg. Chem.* **1998**, *37*, 788.

(31) Rardin, R. L.; Tolman, W. B.; Lippard, S. J. *New J. Chem.* **1991**, *15*, 417.

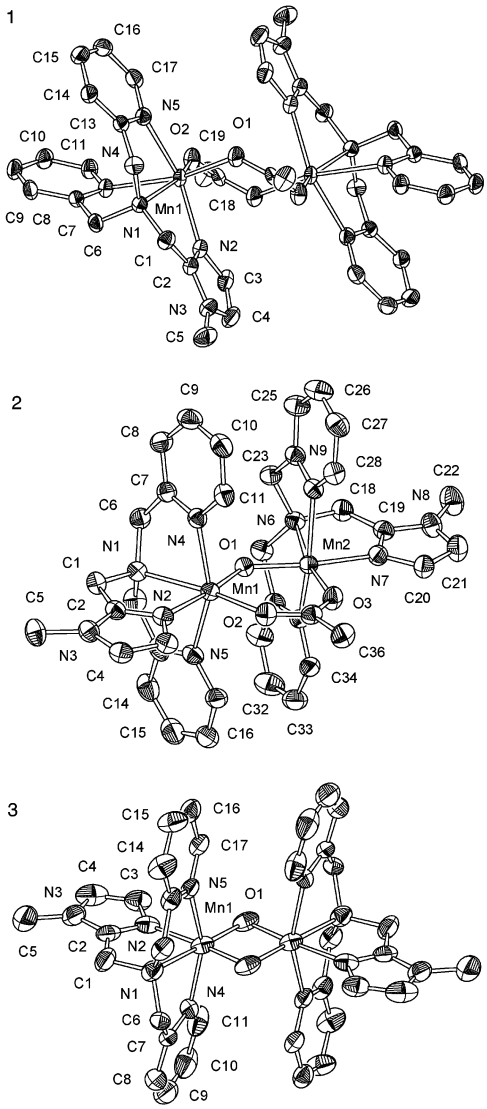

Figure 1. Crystal structures of the cations in **1**, **2**, and **3** showing 50% probability thermal ellipsoids. Hydrogen atoms are omitted for clarity.

environment around the manganese center in **1** is best described as distorted octahedral where four coordination sites are occupied by nitrogen atoms from bpia. It is completed by two oxygen atoms from the bridging acetates. The Mn−N bond distances range from 2.213(2) Å for Mn(1)−N(2) to 2.402(2) Å for Mn(1)−N(1). The distances for the Mn−O bonds are 2.128(2) Å for the anti carboxylate oxygen and 2.087(2) Å for the syn carboxylate oxygen. This difference in bond lengths has been attributed to a higher basicity of the syn carboxylate oxygen compared to the anti carboxylate oxygen.[34] It is noteworthy that the Mn−N bond distances that are trans to the Mn−O bonds are longer than the other Mn−N bond distances (e.g., Mn(1)−N(4) 2.330(2) Å and Mn(1)−N(5) 2.305(2) Å). The distortion of the octahedral coordination environment is manifested in the average N(1)−Mn(1)−N(*X*) (*X* = 2, 4, 5) angle of 73.56° which differs significantly from 90°.

$[Mn_2(bpia)_2(\mu\text{-}O)(\mu\text{-}OAc)](ClO_4)_3\cdot CH_3CN$ (2). The crystal structure of the cation in **2** is depicted in Figure 1. Selected bond distances and angles are given in Table 2. The complex crystallizes in the monoclinic space group $P2_1/n$ with 4 complex cations, 12 perchlorate counteranions, and 4 acetonitrile molecules in the unit cell. The $[Mn_2(\mu\text{-}O)(\mu\text{-}OAc)]^{3+}$ core generates a Mn−Mn distance of 3.2544(8) Å and to our knowledge can be found in only three other crystallographically characterized manganese complexes. In $[Mn_2(bispicen)_2(\mu\text{-}O)(\mu\text{-}OAc)](ClO_4)_3$ (bispicen = *N*,*N*′-bis(2-pyridylmethyl)ethane-1,2-diamine) and $[Mn_2(bispicMe_2en)_2(\mu\text{-}O)(\mu\text{-}OAc)](ClO_4)_3$, the Mn−Mn distances are 3.276(3) and 3.29(1) Å, respectively,[35] while in $[Mn_2(TMIMA)_2(\mu\text{-}O)(\mu\text{-}OAc)](ClO_4)_3\cdot 2CH_3CN$ (TMIMA = tris(1-methylimidazol-2-yl)methyl)amine) the two manganese centers are separated by 3.250(1) Å.[27] The manganese−oxo bond distances Mn(1)−O(1) and Mn(2)−O(1) of 1.785(2) and 1.791(2) Å are consistent with the corresponding bond lengths in the aforementioned compounds. Bonded trans to the oxo group are the imidazole nitrogens N(1) and N(2), with bond lengths of 2.012(2) Å for Mn(1)−N(2) and 2.014(2) Å for Mn(2)−N(7). This is considerably shorter than the manganese−pyridine distances: Mn(1)−N(4) 2.139(2) Å, Mn(1)−N(5) 2.127(2) Å, Mn(2)−N(9) 2.198(2) Å, and Mn(2)−N(10) 2.175(2) Å. The pyridine arms are cis to the oxo group and trans to each other. This shortening of the bond distances along the imidazole nitrogen−manganese−oxo axis is interpreted as a rarely observed Jahn−Teller compression arising from the d^4 configuration of the manganese ions. The distorted octahedral coordination sphere of both manganese centers is completed by the two manganese−acetate bonds Mn(1)−O(2) and Mn(2)−O(3) with distances of 2.028(2) and 1.990(2) Å, respectively, and the two manganese−amine bonds Mn(1)−N(1) and Mn(2)−N(6) with distances of 2.289(2) and 2.223(2) Å, respectively. The average N(1)−Mn(1)−N(*X*) (*X* = 2, 4, 5) and N(6)−Mn(2)−N(*Y*) (*Y* = 7, 9, 10) angles of 77.53° and 77.75° differ significantly from 90° and show the distortion from ideal octahedral geometry due to constraints imposed by the ligand.

$[Mn(bpia)(\mu\text{-}O)]_2(ClO_4)_2(PF_6)\cdot 2CH_3CN$ (3). The crystal structure of the cation in **3** is depicted in Figure 1. Selected bond distances and angles are given in Table 2. Compound **3** crystallizes in the monoclinic space group $P2_1/n$ with two complex cations, four perchlorate and two hexafluorophosphate counteranions, and four acetonitrile molecules in the unit cell. There is a crystallographic inversion center in the middle of the trication, rendering the two halves of the molecule crystallographically equivalent. From the crystallographic data available, it was not possible to determine whether the two halves are chemically equivalent, but the electronic spectrum and the EPR spectrum foster a formulation as a chemically inequivalent valence localized $Mn_2^{III,IV}$ dioxo dimer (vide infra). The manganese centers are bridged

(32) Che, C. M.; Tang, W. T.; Wong, K. Y.; Lai, T. F. *J. Chem. Res., Synop.* **1991**, 30.
(33) Oshio, H.; Ino, E.; Mogi, I.; Ito, T. *Inorg. Chem.* **1993**, *32*, 5697.
(34) (a) Li, Y.; Houk, K. N. *J. Am. Chem. Soc.* **1989**, *111*, 4505. (b) Todayoni, B. M.; Huff, J.; Rebek, J. *J. Am. Chem. Soc.* **1991**, *113*, 2247. (c) Cramer, K. D.; Zimmerman, S. C. *J. Am. Chem. Soc.* **1990**, *112*, 3680. (d) Allen, F. H.; Kirby, A. J. *J. Am. Chem. Soc.* **1991**, *113*, 8829.
(35) Arulsamy, N.; Glerup, J.; Hazell, A.; Hodgson, D. J.; McKenzie, C. J.; Toftlund, H. *Inorg. Chem.* **1994**, *33*, 3023.

Table 2. Selected Bond Distances and Angles for Complexes **1**−**5**

	1	**2**	**3**	**4**	**5**
			Selected Bond Distances (Å)		
Mn(1)−Mn(1A)	4.128(1)	3.2544(8)	2.624(2)		3.5326(9)
Mn(1)−O(1)	2.128(2)	1.785(2)	1.803(5)		1.7663(5)
Mn(1)−O(2)	2.087(2)	2.028(2)	1.824(4)		
Mn(1)−N(1)	2.402(2)	2.289(2)	2.113(6)	2.310(2)	2.313(2)
Mn(1)−N(2)	2.213(2)	2.012(2)	2.010(6)	1.981(2)	2.030(2)
Mn(1)−N(4)	2.330(2)	2.139(2)	2.111(6)	2.084(2)	2.125(2)
Mn(1)−N(5)	2.305(2)	2.127(2)	2.105(5)	2.112(2)	2.093(2)
Mn(1)−Cl(1)				2.2177(9)	2.4065(9)
Mn(1)−Cl(2)				2.3599(9)	
			Selected Angles (deg)		
O(1)−Mn(1)−O(2)	107.37(6)	99.12(8)	87.3(2)		
O(1)−Mn(1)−N_{trans}	160.74(6)	171.80(9)	177.6(2)		171.31(7)
O(2)−Mn(1)−N_{trans}	159.16(6)	168.56(8)	173.1(2)		
N(1)−Mn(1)−N(2)	73.13(6)	79.50(9)	81.7(2)	78.57(8)	77.55(9)
N(1)−Mn(1)−N(4)	74.03(6)	75.97(9)	78.6(2)	76.63(7)	76.99(9)
N(1)−Mn(1)−N(5)	73.53(6)	77.13(9)	78.5(2)	76.36(8)	77.43(9)
N(4)−Mn(1)−N(5)	77.11(7)	152.99(9)	156.2(2)	152.91(8)	154.38(9)
Mn(1)−O(1)−Mn(2)		131.0(1)	92.7(2)		180
Cl(1)−Mn(1)−Cl(2)				98.13(4)	
Cl(1)−Mn(1)−N_{trans}				171.24(6)	165.89(6)

by two oxo groups resulting in a metal−metal separation of 2.624(2) Å and a Mn(1)−O(1)−Mn(1A) angle of 92.7(2)°. The Mn−Mn distance is slightly outside the range of intermanganese distances (2.643−2.738 Å) as well as Mn−O−Mn angles (93.7−97.9°) reported for $Mn^{III,IV}$ dioxo dimers with tripodal all nitrogen donor ligands.[36−39] The bond lengths for Mn(1)−O(1) and Mn(1)−O(1A), 1.803(5) and 1.824(4) Å, are similar to those reported for the aforementioned compounds and also represent an average for the values of 1.78 Å for Mn^{IV} centers and 1.84 Å for Mn^{III} centers in valence localized $Mn^{III,IV}$ dioxo dimers.[37,38] The manganese−imidazole nitrogen bond distance Mn(1)−N(2) trans to the oxo group in **3** of 2.010(6) Å is significantly shorter than the two manganese−pyridine nitrogen bonds that are trans to each other: Mn(1)−N(4) (2.111(6) Å), Mn(1)−N(5) (2.105(5) Å). The manganese−amine bond Mn(1)−N(1) (2.113(6) Å) is only slightly longer than the manganese−pyridine nitrogen bonds. The coordination environment is best described as distorted octahedral. The largest distortion from linearity occurs in the N(4)−Mn(1)−N(5) angle (156.2°), while the deviation from 90° in the average N(1)−Mn(1)−N(*X*) (*X* = 2, 4, 5) angle (79.6°) is less pronounced compared to those of **1** and **2**.

$[Mn(bpia)(Cl)_2](ClO)_4$ (4). The crystal structure of the cation in **4** is depicted in Figure 2. Selected bond distances and angles are given in Table 2. Compound **4** crystallizes in the monoclinic space group *Cc* with four complex cations and four perchlorate counteranions in the unit cell. To our knowledge, this is the first crystallographically characterized Mn^{III} dichloro complex with a tripodal ligand. The corresponding iron complex $[Fe(bpia)(Cl)_2][FeCl_4]$ and related compounds have been described in the literature.[22,40,41] The

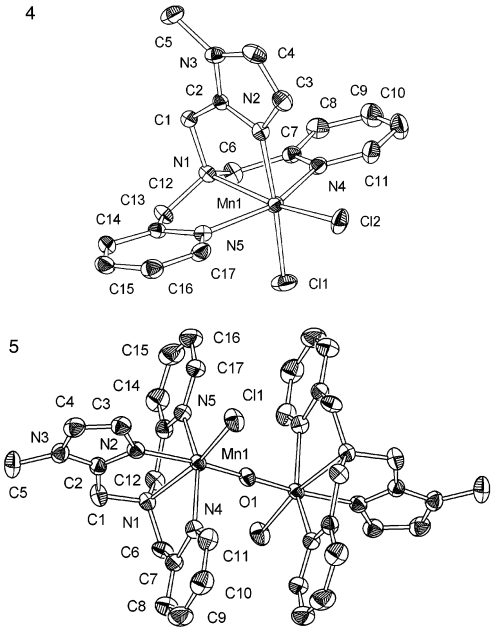

Figure 2. Crystal structures of the cations in **4** and **5** showing 50% probability thermal ellipsoids. Hydrogen atoms are omitted for clarity.

four nitrogen donor atoms of the ligand and the two coordinated chloride ions in **4** provide a distorted octahedral coordination environment. The bond lengths for the manganese−chloride bonds differ significantly from each other, showing values of 2.2177(9) Å for Mn(1)−Cl(1) and 2.3599(9) Å for Mn(1)−Cl(2). The former is similar to the manganese−chloride distance of 2.248(3) Å in $[Mn(phen)_2(Cl)_2]NO_3 \cdot 2.5CH_3COOH$,[42] a Mn^{III} dichloro complex that shows a coordination environment resembling the one in **4**. Trans to Cl(2), the manganese−amine bond Mn(1)−N(1) with a length of 2.310(2) Å can be found, which is longer than the corresponding distances of 2.289(2) Å for Mn(1)−

(36) Schindler, S.; Walter, O.; Pedersen, J. Z.; Toftlund, H. *Inorg. Chim. Acta* **2000**, *303*, 215.
(37) Towle, D. K.; Botsford, C. A.; Hodgson, D. J. *Inorg. Chim. Acta* **1988**, *141*, 167.
(38) Horner, O.; Charlot, M.-F.; Boussac, A.; Anxolabéhère-Mallart, E.; Tchertanov, L.; Guilhem, J.; Girerd, J.-J. *Eur. J. Inorg. Chem.* **1998**, 721.
(39) Oki, A. R.; Glerup, J.; Hodgson, D. J. *Inorg. Chem.* **1990**, *29*, 2435.
(40) Pascaly, M.; Nazzikol, Ç.; Schweppe, F.; Wiedemann, A.; Zurlinden, C.; Krebs, B. *Z. Anorg. Allg. Chem.* **2000**, *626*, 50.
(41) Kojima, T.; Leising, R. A.; Yan, S.; Que, L., Jr. *J. Am. Chem. Soc.* **1993**, *115*, 11328.
(42) Reddy, K. R.; Rajasekharan, M. V. *Polyhedron* **1994**, *13*, 765.

N(1) and 2.223(2) Å for Mn(2)−N(6) in **2** (vide supra). This suggests that the axis Cl(2)−Mn(1)−N(1) is elongated because of Jahn−Teller distortion. The manganese−imidazole nitrogen bond distance Mn(1)−N(2) of 1.981(2) Å trans to Cl(1) is significantly shorter than the two manganese−pyridine nitrogen bonds that are in trans position to each other: Mn(1)−N(4) (2.084(2) Å) and Mn(1)−N(5) (2.112(2) Å). Along the N(4)−Mn(1)−N(5) axis, a large distortion from linearity with an angle of 156.2° occurs which is probably caused by the sterically demanding chloride ligands. Similar to **2**, the average N(1)−Mn(1)−N(*X*) (*X* = 2, 4, 5) angle of 77.19° differs significantly from 90° because of constraints imposed by the ligand.

[(Mn(bpia)(Cl))$_2$(μ-O)](ClO$_4$)$_2$·2CH$_3$CN (5). The crystal structure of the cation in **5** is depicted in Figure 2. Selected bond distances and angles are given in Table 2. Compound **5** crystallizes in the monoclinic space group $P2_1/c$ with two complex cations, four perchlorate counteranions, and four acetonitrile molecules in the unit cell. The oxygen atom O(1) that bridges the two halves of the molecule lies on a crystallographic inversion center, generating a Mn(1)−O(1)−Mn(1A) angle of 180°. The Mn(1)−O(1) bond length of 1.7663(5) Å leads to a Mn(1)−Mn(1A) distance of 3.5326(9) Å. Complex **5** has a distorted octahedral geometry, represented in the trans angles of 165.89(6)° for Cl(1)−Mn(1)−N(1), 171.31(7)° for O(1)−Mn(1)−N(2), and 154.38(9)° for N(4)−Mn(1)−N(5). As has been described for complexes **1**−**4**, the tripodal ligand causes a distortion of the octahedral coordination sphere toward the tertiary amino group that is visible in the average N(1)−Mn(1)−N(*X*) (*X* = 2, 4, 5) angle of 77.32°. The complexes [(Fe(tpa)(Cl))$_2$(μ-O)](ClO$_4$)$_2$ and [(Mn(L^2))$_2$(μ-O)](ClO$_4$)$_2$ (L^2 = *N*,*N*-bis(2-pyridylmethyl)-*N*′-(2-hydroxybenzyl)ethane-1,2-diamine) also contain a single oxo bridge with the bridging oxygen atom on a crystallographic inversion center.[41,43] The intermetal distances of 3.581(2) and 3.516 Å (calculated from the Mn−oxo bond distance) resemble the one found in **5**. While for [(Mn(L^2))$_2$(μ-O)](ClO$_4$)$_2$ a Jahn−Teller distortion along the pyridine−manganese−pyridine axis is reported, the coordination environment in **5** is similar to that in **4**. The longest bonds in **5** are Mn(1)−Cl(1) and Mn(1)−N(1) with distances of 2.4065(9) and 2.313(2) Å, where the former is trans to the latter. This suggests that the Jahn−Teller distortion leads to an elongation of the Cl(1)−Mn(1)−N(1) axis. The manganese−pyridine bonds, which are trans to each other, show values of 2.125(2) Å for Mn(1)−N(4) and 2.093(2) Å for Mn(1)−N(5), while the manganese−imidazole bond distance Mn(1)−N(2) is 2.030(2) Å.

Electronic Spectra. The electronic spectra of complexes **2**−**5** are depicted in Figure 3. Bands and extinction coefficients are summarized in Table T26 (Supporting Information). The UV−vis spectrum of **1** shows no bands. This is similar to the optical spectrum of manganese catalase from *Thermus thermophilus* (TTC) in the (II,II) oxidation state, which lacks any visible absorption.[44] For **2**, bands can be found at 495 nm (524 L·mol^{-1}·cm^{-1}) and 527 nm (418 L·mol^{-1}·cm^{-1}) which are assigned to d−d transitions.[35,45] A broad absorption feature is centered at 711 nm (176 L·mol^{-1}·cm^{-1}). This is analogous to the UV−vis spectra reported for the aforementioned complexes [Mn$_2$(TMIMA)$_2$(μ-O)(μ-OAc)](ClO$_4$)$_3$·2CH$_3$CN and [Mn$_2$(bispicen)$_2$(μ-O)(μ-OAc)](ClO$_4$)$_3$.[27,35] The spectrum of **2** resembles the one reported for manganese catalase from *Thermus thermophilus* (TTC) in the (III,III) oxidation state with a band at 492 nm and a broad tail going into the near-IR region.[44] The spectrum of **3** exhibits a shoulder at 382 nm (1710 L·mol^{-1}·cm^{-1}) and three bands at 442 nm (1300 L·mol^{-1}·cm^{-1}), 557 nm (610 L·mol^{-1}·cm^{-1}), and 647 nm (502 L·mol^{-1}·cm^{-1}); the features are comparable to those of other Mn$_2^{III,IV}$O$_2$ compounds.[35,36,39] Especially, the latter three absorptions are in very good accordance with the UV−vis bands of 433, 555, and 654 nm reported for the [Mn(*N*,*N*-bispicen)(μ-O)]$_2^{3+}$ system (*N*,*N*-bispicen = *N*,*N*-bis(2-pyridylmethyl)-1,2-diaminoethane).[38] Therefore, the following assignments for the bands in **3** are made:[46] the absorption at 442 nm is attributed to partial contributions of LMCT oxo Mn^{IV} and Mn^{IV} d−d transitions, and the band at 557 nm corresponds to a Mn^{IV} d−d transition while the one at 654 nm originates from a LMCT oxo Mn^{IV} transition. Because the [Mn(*N*,*N*-bispicen)(μ-O)]$_2^{3+}$ system contains a crystallographically inequivalent Mn$_2^{III,IV}$O$_2$ core, the similarity of the two spectra is an indication that **3** is only crystallographically but not chemically equivalent. Furthermore, similarities between the UV−vis spectra of **3** and the superoxidized form of manganese catalase from *Lactobacillus plantarum* (LPT) can be found. LPT exhibits bands at 362 nm (1680 L·mol^{-1}·cm^{-1}), 442 nm (928 L·mol^{-1}·cm^{-1}), and 621 nm (320 L·mol^{-1}·cm^{-1}).[46] These bands match the shoulder and two of the three bands in **3**. The spectrum of complex **4** exhibits a shoulder at 379 nm (902 L·mol^{-1}·cm^{-1}) and a band at 514 nm (512 L·mol^{-1}·cm^{-1}). Comparison with [Fe(tpa)(Cl)$_2$](ClO$_4$)[41] and [Fe(bpia)(Cl)$_2$][FeCl$_4$][22] suggests an assignment of the shoulder as an LMCT chloro Mn^{III} transition. The band in the visible region is attributed to a Mn^{III} d−d transition.[45] The

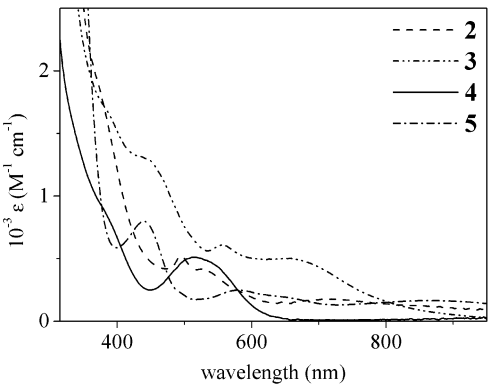

Figure 3. Electronic spectra of complexes **2**−**5**.

(43) Horner, O.; Anxolabéhère-Mallart, E.; Charlot, M.-F.; Tchertanov, L.; Guilhem, J.; Mattioli, T. A.; Boussac, A.; Girerd, J.-J. *Inorg. Chem.* **1999**, *38*, 1222.

(44) Whittaker, M. M.; Barynin, V. V.; Antonyuk, S. V.; Whittaker, J. W. *Biochemistry* **1999**, *38*, 9126.

(45) Dingle, R. *Acta Chem. Scand.* **1966**, *20*, 33.

(46) Gamelin, D. R.; Kirk, M. L.; Stemmler, T. L.; Pal, S.; Armstrong, W. H.; Penner-Hahn, J. E.; Solomon, E. I. *J. Am. Chem. Soc.* **1994**, *116*, 2392.

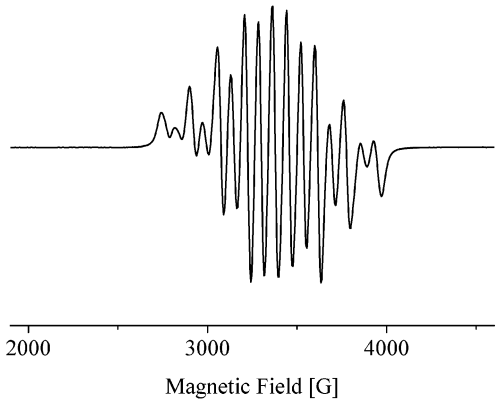

Figure 4. EPR spectrum of **3** in acetonitrile (22 K).

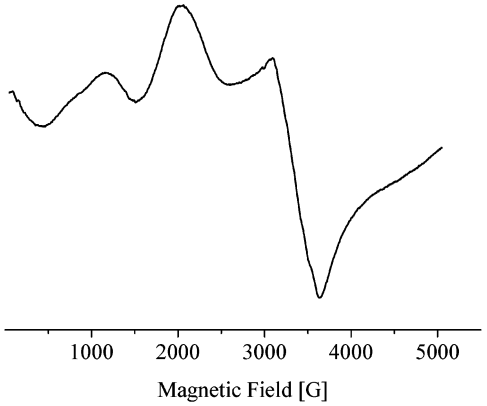

Figure 5. EPR spectrum of **1** in *N*,*N*-dimethylformamide (4 K).

UV−vis spectrum of **5** reveals three absorptions, one band at 439 nm (800 L·mol^{-1}·cm^{-1}), one broadened band at 581 nm (250 L·mol-^{1}·cm^{-1}), and a broad absorption centered at 865 nm (164 L·mol^{-1}·cm^{-1}). When compared to the only other spectrum reported for a $Mn^{III}-O-Mn^{III}$ complex, noticeable differences are found. $[(Mn(L^2))_2(\mu\text{-}O)](ClO_4)_2$ (vide supra) gives a spectrum with bands at 300 nm (21000 L·mol^{-1}·cm^{-1}), 400 nm (4800 L·mol^{-1}·cm^{-1}), and 500 nm (1000 L·mol^{-1}·cm^{-1}).[43] These differences are likely to be due to the different coordination environments of manganese in the two complexes (imine nitrogen/phenolate oxygen in $[(Mn(L^2))_2(\mu\text{-}O)](ClO_4)_2$ versus imidazole nitrogen/chloride in **5**).

EPR Spectroscopy. A frozen solution (22 K) of complex **3** in acetonitrile exhibits an EPR signal with 16 nuclear hyperfine lines centered at $g = 2.02$ (Figure 4). This spectrum is characteristic of the $Mn_2^{III,IV}O_2$ core with an $S = {}^1/_2$ ground state that arises from antiferromagnetic coupling of a Mn^{III} nucleus with a Mn^{IV} nucleus, which suggests that the nuclei in this compound are valence localized. The average hyperfine coupling constant for **3** is $A = 79$ G. Similar spectra for analogous compounds have been reported in the literature.[28,36,38,39] For complex **1**, EPR spectra have been recorded in different solvents. In a frozen methanol solution (77 K), **1** exists as a mononuclear Mn^{II} species indicated by the six line signal centered at $g = 2.02$ with a hyperfine coupling constant of $A = 90$ G, a pattern typical for this type of compound (Figure F1a, Supporting Information). EPR measurements of **1** in a frozen *N*,*N*-dimethylformamide solution (4 K) yield a different result (Figure 5). In this case, a spectrum with one broad absorption centered at $g = 5.77$ and another one centered at $g = 3.26$ showing a hyperfine coupling constant of $A = 50$ G is obtained. This coupling constant differs from the value of 90 G for the mononuclear species (vide supra). These differences in A values indicate that **1** is not a mononuclear species but exists as a $Mn_2^{II,II}$ dimer. To further prove the dinuclear nature of **1**, temperature-dependent EPR studies have been performed (Figure F1b). When the temperature is raised, in addition to the above-mentioned signals, a new six line signal centered at $g \approx 2.0$ with hyperfine coupling constants ranging from 95 to 104 G emerges. This new signal is caused by a small impurity (<5%) of a mononuclear Mn^{II} species (vide supra). Therefore, the signals at $g = 5.77$ and 3.26 correspond to dinuclear species **1**. The formulation of **1** as a dimer is supported by comparison with the EPR spectra of several other dinuclear $Mn_2^{II,II}$ complexes.[17,47]

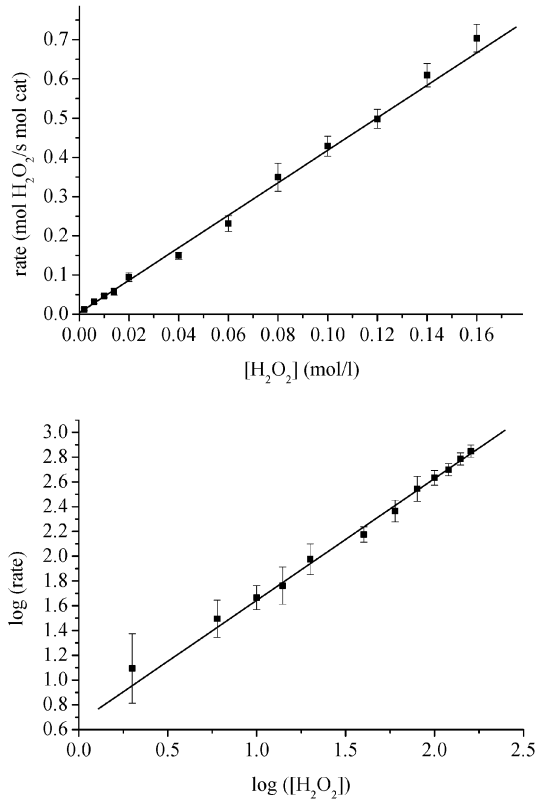

Figure 6. Initial rate of substrate consumption versus substrate concentration (top) and double logarithmic plot of initial rate of substrate consumption versus substrate concentration (bottom) at constant concentration of **3** (196 mM).

Electrochemistry. Cyclic voltammograms for complexes **2**−**5** are depicted in Figure F2. Redox potentials are summarized in Table T27. All values are given versus SCE.

(47) (a) Howard, T.; Telser, J.; DeRose, V. J. *Inorg. Chem.* **2000**, *39*, 3379. (b) Sun, L.; Raymond, M. K.; Magnuson, A.; LeGourriérec, D.; Tamm, M.; Abrahamsson, M.; Kenéz, P. H.; Martensson, J.; Stenhagen, G.; Hammarström, L.; Styring, S.; Akermark, B. *J. Inorg. Biochem.* **2000**, *78*, 15−22. (c) Boelrijk, A. E. M.; Khangulov, S. V.; Dismukes, G. C. *Inorg. Chem.* **2000**, *39*, 3009. (d) Khangulov, S. V.; Pessiki, P. J.; Barynin, V. V.; Ash, D. E.; Dismukes, G. C. *Biochemistry* **1995**, *34*, 2015. (e) Kessissoglou, D. P.; Butler, W. M.; Pecoraro, V. L. *Inorg. Chem.* **1987**, *26*, 495.

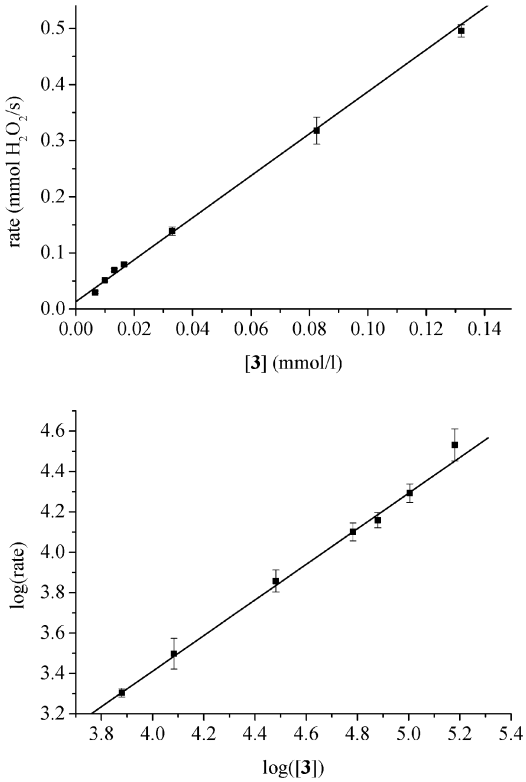

Figure 7. Initial rate of substrate consumption versus concentration of **3** (top) and double logarithmic plot of initial rate of substrate consumption versus concentration of **3** (bottom) at constant substrate concentration (20 mM).

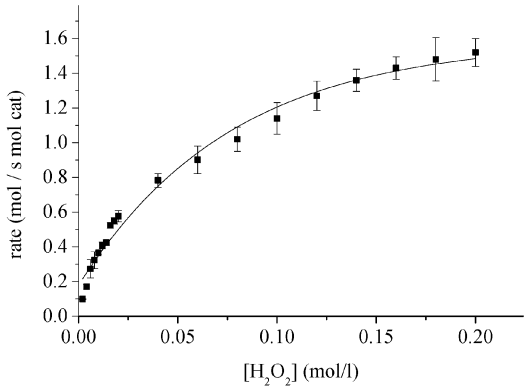

Figure 8. Initial rate of substrate consumption versus substrate concentration at constant concentration of **1** (■ indicates data points, — indicates curve fit).

In *N*,*N*-dimethylformamide solution, complex **1** displays a quasireversible one electron redox process at $E_{1/2} = 0.65$ V with $\Delta E = 140$ mV, corresponding to the $Mn_2^{II,II}/Mn_2^{II,III}$ redox couple. The cyclic voltammogram of **2** shows three redox processes. The wave couple at $E_{1/2} = 0.13$ V originates from the $Mn_2^{II,III}/Mn_2^{III,III}$ redox couple and is quasireversible. The peaks are separated by 200 mV. For the two quasireversible transitions at potentials of $E_{1/2} = 0.98$ V and $E_{1/2} = 1.20$ V, the peak separations amount to 70 and 170 mV, respectively. They are tentatively assigned to the $Mn_2^{III,III}/Mn_2^{III,IV}$ and $Mn_2^{III,IV}/Mn_2^{IV,IV}$ couples. These results differ from the electrochemical behavior reported for the structurally similar compound $[Mn_2(TMIMA)_2(\mu\text{-O})(\mu\text{-OAc})](ClO_4)_3 \cdot 2CH_3CN$.[27] This complex exhibits an irreversible

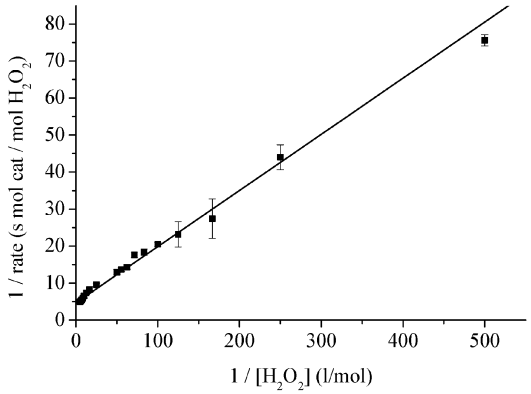

Figure 9. Lineweaver−Burk plot for **1**.

peak for the reduction $Mn^{III,III}/Mn^{II,III}$ at $E_{1/2} = -0.12$ V. At $E_{1/2} = 1.00$ V ($\Delta E = 340$ mV), an irreversible redox process is observed and attibuted to the $Mn^{III,III}/Mn^{III,IV}$ couple. Another redox step is found at $E_{1/2} = 1.58$ V, which is quasireversible ($\Delta E = 70$ mV). The half wave potentials for the $Mn_2^{III,III}/Mn_2^{III,IV}$ and $Mn_2^{III,IV}/Mn_2^{IV,IV}$ redox couples in **3** are $E_{1/2} = 0.23$ V ($\Delta E = 80$ mV) and $E_{1/2} = 1.10$ V ($\Delta E = 140$ mV), respectively. The values for these quasireversible steps are in good accordance with potentials reported previously for similar complexes.[28,36,38,39] The cyclic voltammogram of complex **4** exhibits two quasireversible redox processes at $E_{1/2} = 0.61$ V ($\Delta E = 90$ mV) and $E_{1/2} = 1.53$ V ($\Delta E = 90$ mV) for the Mn^{II}/Mn^{III} and the Mn^{III}/Mn^{IV} couples, respectively. The $Mn_2^{II,III}/Mn_2^{III,III}$, $Mn_2^{III,III}/Mn_2^{III,IV}$, and $Mn_2^{III,IV}/Mn_2^{IV,IV}$ quasireversible redox couples of complex **5** have values of $E_{1/2} = 0.63$ V ($\Delta E = 80$ mV), $E_{1/2} = 1.09$ V ($\Delta E = 80$ mV), and $E_{1/2} = 1.54$ V ($\Delta E = 90$ mV). These values are shifted to more positive potentials with respect to the corresponding redox couples of complex **2**. Formally, two oxygen donor atoms from the bridging carboxylate ligand in **2** have been replaced with chloride in **5** while the remaining donor set and the oxidation state have been retained. With an alteration from a bent oxo bridge to a linear oxo bridge, only minor structural changes occur. Therefore, the shift of the redox potentials to more positive values is attributed to ligated chloride. This result is supported by the comparison of the Mn^{III}/Mn^{IV} redox couple of **4** with the $Mn_2^{III,III}/Mn_2^{III,IV}$ redox couple of **5**. The more positive value for **4** (1.53 V compared to 1.09 V for **5**) is consistent with the formal substitution of a [Mn(bpia)(Cl)(μ-O)] fragment with chloride in **5**. For $[(Mn(L^2))_2(\mu\text{-O})](ClO_4)_2$, the only other $Mn_2^{III,III}O$ complex with a single unsupported oxo bridge reported so far, a different electrochemical behavior is observed.[43] The potentials for the reversible $Mn_2^{III,III}/Mn_2^{III,IV}$ and $Mn_2^{III,IV}/Mn_2^{IV,IV}$ redox steps are significantly more negative, namely $E_{1/2} = 0.54$ V and $E_{1/2} = 0.99$ V, respectively. Furthermore, an irreversible reduction wave is found at a peak potential of $E = -0.69$ V.

Catalase Activity. Compounds **1**−**5** are stable under ambient conditions and are not oxidized by atmospheric dioxygen. Upon addition of hydrogen peroxide to solutions of complexes **4** and **5** in acetonitrile, these are reduced. Even with a large excess of hydrogen peroxide present, reoxidation does not occur. Furthermore, the reduced forms of **4** and **5**

Table 3. Catalytic Activity of Manganese Catalases and Synthetic Catalase Mimics

cmpd	k_{cat} (s^{-1})	K_M (mM)	k_{cat}/K_M ($s^{-1}\cdot M^{-1}$)	ref
T. thermophilus catalase	2.6×10^5	83	3.1×10^6	49
L. plantarum catalase	2.0×10^5	350	0.6×10^6	50
T. album catalase	2.6×10^4	15	1.7×10^6	7
$[Mn(bpia)(\mu\text{-}OAc)]_2(ClO_4)_2$ (**1**)	1.1×10^3	31.5	3.4×10^4	this work
$[Mn(salpn)O]_2$	2.5×10^2	250	1×10^3	51, 52
$[Mn_2(2\text{-}OHsalpn)_2]$	4.2−21.9	10.2−118.0	160−990	19, 20
$[Mn_2(tacn)(bpy)(\mu\text{-}O)_2(\mu\text{-}OAc)(MeOH)](ClO_4)_2\cdot MeOH$	13.2[a]			53[c]
$[Mn(bpia)(\mu\text{-}O)]_2(ClO_4)_2\text{-}(PF_6)\cdot 2CH_3CN$ (**3**)	8.1[a]			this work
$[Mn_2(tacn)(\mu\text{-}O)_2(\mu\text{-}OAc)(OAc)_2]$	5.5[a]			53[c]
$[Mn_2(L^1)(\mu\text{-}OAc)(H_2O)]^{2+}$	2.1[a]	0.3	700	15−18[b]
$[Mn_2(salpentO)(\mu\text{-}OAc)\text{-}(\mu\text{-}OMe)(MeOH)_2]$	0.66	36	18	48
$[Mn(H_2O)_6](ClO_4)_2$	0.0063[a]			19

[a] No saturation kinetics observed/reported. [b] L^1 = *N,N,N′,N′*-tetrakis(2-methylenebenzimidazolyl)-1,3-diaminopropan-2-ol. [c] tacn = 1,4,7-trimethyl-1,4,7-triazacyclononane, bpy = 2,2′-bipyridine.

show no ability to disproportionate hydrogen peroxide. No gas evolution can be observed under the conditions described previously. In contrast to this, the reaction of **2** with hydrogen peroxide yields gas evolution accompanied by a color change of the complex solution from red to green. The UV spectrum of the product solution is identical to the one for complex **3** indicating that **2** has been oxidized by one electron to yield **3**. Because complex **3** itself is an effective catalyst for the disproportionation of hydrogen peroxide (vide infra) and compounds **2** and **3** are both present in solution, a determination of the catalase activity of **2** with the method employed is not possible. Complex **3**, although being a structural model for the catalytically inactive "superoxidized" form of manganese catalases, is a catalyst for the disproportionation of hydrogen peroxide in acetonitrile solution. A linear dependence of the initial rate of substrate consumption versus the substrate concentration at a constant catalyst concentration (196 mM) is observed for **3** for the range 10-fold to 800-fold excess of substrate over catalyst (Figure 6). With the experimental setup employed, measurements at either a higher or lower excess of hydrogen peroxide over catalyst are not feasible. At a constant substrate concentration (20 mM), the initial rate of substrate consumption versus catalyst concentration is also linear (Figure 7). Figures 6 and 7 present these data in double logarithmic plots. Linear relationships with slopes of 0.98 ± 0.03 for varying substrate concentration and 0.88 ± 0.02 for varying catalyst concentration are obtained, confirming a first order dependence of the reaction in substrate and catalyst. An initial rate constant of $k_0 = (8.1 \pm 0.3)\ s^{-1}$ has been extracted from the plots. This result is similar to the range of values for $k_{cat} = 4.2-21.9\ s^{-1}$ obtained for the $[Mn_2(2\text{-}OHsalpn)_2]$ catalase model system, which shows saturation kinetics.[19,20] Values for K_M between 10.2 and 118.0 mM and for k_{cat}/K_M between 160 and 990 $s^{-1}\cdot M^{-1}$ have been determined. A comparable activity with a $k_{cat}/K_M = 700\ s^{-1}\cdot M^{-1}$, based on this criterion, has been reported for the $[Mn_2(L^1)(\mu\text{-}OAc)(H_2O)]^{2+}$ (vide supra) system. The values of $k_{cat} = 2.1\ s^{-1}$ and $K_M = 0.3$ mM, however, are much lower.[15] Another set of binuclear manganese complexes based on the pentadentate ligand salpentOH has been reported to exhibit Michaelis−Menten kinetics for the catalytic disproportionation of hydrogen peroxide, albeit with lower activity. For $[Mn_2(salpentO)(\mu\text{-}OAc)(\mu\text{-}OMe)(MeOH)_2]$, values of $k_{cat} = (0.66 \pm 0.06)\ s^{-1}$, $K_M = (36 \pm 3)$ mM, and $k_{cat}/K_M = 18\ s^{-1}\cdot M^{-1}$ have been obtained.[48] Complex **1**, which can be considered as a structural model for the catalytically active reduced form of manganese catalases, is a rare example of a synthetic catalyst for the disproportionation of hydrogen peroxide (in *N*-methylformamide) showing saturation kinetics at high substrate concentrations (Figure 8). Consequently, the data were fit to the Michaelis−Menten equation, and the turnover number $k_{cat} = (10.7 \pm 0.5)\cdot 10^2\ s^{-1}$, the Michaelis constant $K_M = (31.5 \pm 3.6$ mM), and $k_{cat}/K_M = (34.0 \pm 5.5)\cdot 10^3\ M^{-1}\cdot s^{-1}$ were determined from the double reciprocal Lineweaver−Burk plot (Figure 9). This places complex **1** within 2−3 orders of magnitude relative to the three characterized manganese catalases (*Thermus thermophilus*, *Thermoleophilum album*, *Lactobacillus plantarum*) on both k_{cat} and k_{cat}/K_M criteria. Table 3 summarizes the activities of the native enzymes and selected synthetic catalase mimics.

Conclusion. With the tripodal ligand bpia (bis(picolyl)-(*N*-methylimidazol-2-yl)amine), a structural, spectroscopic, and functional model system for manganese catalases has been synthesized and structurally characterized. Model complexes for the catalytically active $Mn_2^{II,II}$, $Mn_2^{III,III}$ oxidation states and the so-called superoxidized $Mn_2^{III,IV}$ state of the enzyme have been obtained. Attempts to prepare an analogous compound in the $Mn_2^{II,III}$ oxidation state have not been successful. $[Mn(bpia)(\mu\text{-}OAc)]_2(ClO_4)_2$ (**1**) and $[Mn(bpia)(\mu\text{-}O)]_2(ClO_4)_2(PF_6)\cdot 2CH_3CN$ (**3**) are the most efficient catalysts using the $Mn_2^{II,II}$ to $Mn_2^{III,III}$ redox couple reported to date for the disproportionation of hydrogen peroxide, while $[Mn_2(bpia)_2(\mu\text{-}O)(\mu\text{-}OAc)](ClO_4)_3\cdot CH_3CN$

(48) Palopoli, C.; Chansou, B.; Tuchagues, J.-P.; Signorella, S. *Inorg. Chem.* **2000**, *39*, 1458.
(49) Shank, M.; Barynin, V.; Dismukes, G. C. *Biochemistry* **1994**, *33*, 15433.
(50) Penner-Hahn, J. In *Manganese Redox enzymes*; Pecoraro,V. L., Ed.; VCH Publishers: New York, 1992; pp 29−45.
(51) Rosenzweig, A. C.; Frederick, C. A.; Lippard, S. J.; Nordlund, P. *Nature* **1993**, *366*, 537.
(52) Larson, E. J.; Pecoraro, V. L. *J. Am. Chem. Soc.* **1991**, *113*, 7809.
(53) Bossek, U.; Saher, M.; Weyhermüller, T.; Wieghardt, K. J. *J. Chem. Soc., Chem. Commun.* **1992**, 1780.

(**2**) is rapidly oxidized by hydrogen peroxide. The chloride complexes $[Mn(bpia)(Cl)_2](ClO)_4$ (**4**) and $[(Mn(bpia)(Cl))_2(\mu\text{-}O)](ClO_4)_2 \cdot 2CH_3CN$ (**5**) can be regarded as functional mimics for the halide inhibited forms of the native enzyme.

Acknowledgment. Financial support by the DFG (Deutsche Forschungsgemeinschaft) and by the COST program of the European Union is gratefully acknowledged. M.U.T. thanks the FCI (Fonds der Chemischen Industrie) for a Doktorandenstipendium. V.L.P. thanks the NIH (GM39406) and the Alexander von Humboldt award for senior U.S. scientists for financial support. A.R. thanks the MSWF for the Bennigsen-Foerder-Preis.

Supporting Information Available: EPR spectrum of **1** in methanol, cyclic voltammograms of complexes **2**−**5**, table of UV−vis bands, table of redox potentials, tables containing atomic coordinates and equivalent isotropic displacement parameters, bond lengths, angles, anisotropic displacement parameters, hydrogen coordinates and isotropic displacement parameters, crystal data, and X-ray experimental parameters for complexes **1**−**5** and crystallographic data in CIF format. This material is available free of charge via the Internet at http://pubs.acs.org.

IC025897A